2015 IEEE/RSJ International Conference on Intelligent Robots and Systems (IROS)
Congress Center Hamburg
Sept 28 - Oct 2, 2015. Hamburg, Germany

Computational Modeling of N-body Collisions

Feifei Wang, Huan Lin, and Yan-Bin Jia
Department of Computer Science
Iowa State University
Ames, IA 50011, USA
wangff, linhuan, jia@iastate.edu

***Abstract*— This paper presents an impulse-based model for n-body collisions with or without friction. In the frictionless case, impulses at all the contacts, initialized via solution of a non-linear system, accumulate over different phases (compression and restitution) tracked through numerical integration. Experiment over Newton's cradle, using vision-based velocity estimation, achieves a close agreement with simulation. The presence of friction requires a contact mode analysis via solution of a linear system to check for contact mode consistencies with Coulomb's friction law. Simulation of nine-ball break shots, drawing upon a recent trajectory study [6], yields realistic scenarios. The modeling approach is part of our efforts toward planning for robotic manipulation strategies using impulsive forces.**

I. Introduction

Multi-body collision is a common phenomenon that takes place when several objects collide together, as observed in the games of marbles, billiards, and bowling. To make the robot purposefully take advantage of impact to quickly carry out certain tasks, a general and computationally efficient model is needed for predicting the outcome of an n-body collision.

Impact occurs over a short period of time, generating a very large interaction force. Constraint-based and penalty-based approaches cannot model the wave effect of multi-body impact. Such effect is exhibited in the velocity profile during the impact, and unless well modeled, could lead to a poor match of simulation results against what we actually observe. In the past, little work has been done on impulsive manipulation. Noticeable results include [4], [13], [3] and [14]. Recent work by the third author [7] modeled contacts during a multi-body collision as virtual springs, with a focus on three-body impact, and described the entire process as a diagram showing different periods that transition into one and another. This model in theory can be extended to predict the outcome of collision with any numbers of bodies involved, when combined with his study [5] of tangential impulse under compliance. However, a general framework and related computational issues still need to be worked out.

In this paper, we will introduce an n-body impulse-based collision model that works with or without friction. The model can be used to determine the post-collision motions of any number of objects engaged in the collision. Our focus will be on the case where the centers of mass of the objects engaged in the collision are coplanar. At the conclusion of the paper, we will discuss how the model can be readily extended to a general collision configuration.

Section II adopts the idea from [7] to set up a system for frictionless collisions of n balls. Angular velocities are not considered for the moment. During a collision process, impulses and energies at various contacts are tracked via numerical integration based on their differential relationships to the dominant impulse, which switches from one contact to another. To initialize the impulse derivatives, instead of using wave propagation [8] and [9], we set up a system of equations and solve it numerically using Newton's method. This avoids enumeration of all possible propagation scenarios during the collision. An energetic coefficient of restitution [12] is employed to track the energy loss. Our model is then used to simulate Newton's cradle, in which no rotation is involved and friction between the balls is negligible. The problem was studied earlier [2, 1] by considering coupling effects via the use of an impulse correlation ratio.

Section III considers friction and the angular velocities of n rigid objects with arbitrary shapes involved in the collision. Tangential impulse, now existing at every contact, has to be determined. This requires an analysis of the sticking and sliding modes under Coulomb's law of friction. We are then able to set up the differential relationship between the tangential and normal impulses at every contact.

In Section IV, we first conduct simulation and experiment on Newton's cradle to validate the model for frictionless n-body collision. Next, we apply the frictional collision model to simulate nine-ball break shots. It is noteworthy that work [17, 16] has been done on simulations and experimental validations on dynamics of planar objects when Coulomb's friction is

978-1-4799-9993-4/15/$31.00 ©2015 IEEE

present, such as bouncing dimer or rocking blocks.

The final section offers a brief summary of the paper, and outlines some future work to improve the efficiency and further validate the model's accuracy.

II. Frictionless Collision of Translating Balls

In this section, we investigate a frictionless collision among n translating balls whose centers of mass are coplanar. The difference between our model and [8] is that they do not explicitly handle multiple objects using a graph representation, and the initialization there is based on propagation rather than solution of a system of equations. The issues with [8] no longer exist in our initialization scheme. This model is then applied to solve Newton's Cradle problem.

A. Impact dynamics and contact kinematics

Suppose that n rigid balls $\mathcal{B}_1, \ldots, \mathcal{B}_n$ are engaged in a collision. Let $\boldsymbol{v}_i$ be the velocity of $\mathcal{B}_i$, $\boldsymbol{I}_{ij}$ be the impulse that $\mathcal{B}_i$ receives from $\mathcal{B}_j$. By Newton's third law, $\boldsymbol{I}_{ij} = -\boldsymbol{I}_{ji}$. For $1 \le i \le n$, denote $\mathbb{C}_i$ as the set of subscripts of the objects that are in contact with $\mathcal{B}_i$, which has initial velocity $\boldsymbol{v}_i^{(0)}$. Then the velocity of $\mathcal{B}_i$ during the collision changes as follows:

$$\boldsymbol{v}_i \;=\; \boldsymbol{v}_i^{(0)} + \frac{1}{m_i}\sum_{k\in\mathbb{C}_i} \boldsymbol{I}_{ik}, \quad i = 1, 2, ..., n. \quad (1)$$

For every two balls $\mathcal{B}_i$ and $\mathcal{B}_j$ in contact, we add a virtual spring $\{i, j\}$ at the contact point. Without ambiguity, we will also refer to the contact by the same notation $\{i, j\}$. This spring is along the contacting normal which is perpendicular to their common tangent plane. Fig. 1 shows the ball $\mathcal{B}_i$ with the contact set $\mathbb{C}_i = \{j_1, j_2, j_3\}$. Impulsive forces on the balls are much

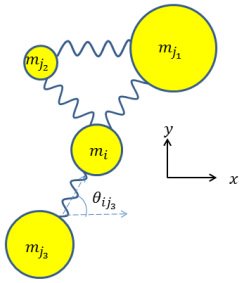

Fig. 1: Contact modeling with virtual springs.

larger than the gravitational forces, which can be ignored consequently. Reorient the system such that all the balls lie on a horizontal plane. For the spring $\{i, j\}$, let θ_{ij} be the angle from the x-axis to the spring direction vector, which points from $\mathcal{B}_j$ to $\mathcal{B}_i$ if $j > i$, and in the opposite direction otherwise. Thus, the unit normal vector $\hat{\boldsymbol{n}}_{ij} = (\cos\theta_{ij}, \sin\theta_{ij})$ always points from the ball with the bigger subscript to the ball with the smaller one. We let $I_{ij} = \sigma_{ij}\|\boldsymbol{I}_{ij}\|$, where $\sigma_{ij} = 1$ when $i < j$, and -1 when $i > j$. The velocity components of ball $\mathcal{B}_i$ during impact can then be written as:

$$\begin{pmatrix} v_{ix} \\ v_{iy} \end{pmatrix} \;=\; \begin{pmatrix} v_{ix}^{(0)} \\ v_{iy}^{(0)} \end{pmatrix} + \frac{1}{m_i}\sum_{k\in\mathbb{C}_i} \begin{pmatrix} I_{ik}\cos\theta_{ik} \\ I_{ik}\sin\theta_{ik} \end{pmatrix}. \quad (2)$$

Denote $\mathbb{P}$ as the set of contacts, and $\tilde{v}_{ij}$ as $\mathcal{B}_i$'s velocity component projected onto the direction of the spring $\{i, j\}$. For every contact $\{i, j\} \in \mathbb{P}$, we thus have $\tilde{v}_{ij} = \boldsymbol{v}_i \cdot \hat{\boldsymbol{n}}_{ij}$. Let x_{ij} be the change in length of the virtual spring $\{i, j\}$, and k_{ij} as its stiffness. The derivative of energy with respect to its impulse follow from $\tilde{v}_{ij}$ and equation (1):

$$\frac{dE_{ij}}{dI_{ij}} = -\dot{x}_{ij} = \tilde{v}_{ji} - \tilde{v}_{ij} = \left(\boldsymbol{v}_j^{(0)} - \boldsymbol{v}_i^{(0)}\right)\cdot\hat{\boldsymbol{n}}_{ij} + \frac{1}{m_j}\sum_{k\in\mathbb{C}_j} I_{jk}(\hat{\boldsymbol{n}}_{jk}\cdot\hat{\boldsymbol{n}}_{ij}) - \frac{1}{m_i}\sum_{k\in\mathbb{C}_i} I_{ik}(\hat{\boldsymbol{n}}_{ik}\cdot\hat{\boldsymbol{n}}_{ij}). \quad (3)$$

The potential energy stored in the spring $\{i, j\}$ is $E_{ij} = \frac{1}{2}k_{ij}x_{ij}^2$, and the formula for the contact force by Hooke's law is $F_{ij} = k_{ij}x_{ij}$. Suppose the spring $\{p, q\}$ accumulates the primary impulse I_{pq}, which has the largest growth during the period. The expression of dE_{pq}/dI_{pq} is given by (3) after replacing i, j with p, q. Then, the differential ratio between I_{ij} and I_{pq} can be derived as

$$\rho_{ij} = \frac{dI_{ij}}{dI_{pq}} = \frac{F_{ij}}{F_{pq}} = \sigma_{ij}\sigma_{pq}\sqrt{\frac{k_{ij}E_{ij}}{k_{pq}E_{pq}}}. \quad (4)$$

Integrate equation (3) from $I_{ij}^{(0)} = \rho_{ij}I_{pq}^{(0)}$ to $\rho_{ij}(I_{pq}^{(0)} + \delta)$ gives the major part of the accumulated change of energy ΔE_{ij}, where δ is the increment of the primary impulse I_{pq}. An extra term $\alpha_{ij}(e_{ij}^2 - 1)E_{ijmax}$ needs to be added after the integration, where $e_{ij} \in [0, 1]$ is the coefficient of restitution determined by the material properties of the two impacting objects. After the spring finishes compression, it starts to restitute, with the stiffness k_{ij} adjusted to k_{ij}/e_{ij}^2 to reflect material hardening as explained in [7]. The value of α_{ij} is set to be 0 during compression and 1 during restitution. At the end of compression, the spring stores the maximum energy E_{ijmax}, and then immediately loses a portion of $1 - e_{ij}^2$. We can work out the integrals below:

$$\int_{\rho_{ij}I_{pq}^{(0)}}^{\rho_{ij}(I_{pq}^{(0)}+\delta)} \Delta I_{ik}\, dI_{ij} = c\rho_{ij}\rho_{ik}, \quad (5)$$

$$\int_{\rho_{ij}I_{pq}^{(0)}}^{\rho_{ij}(I_{pq}^{(0)}+\delta)} \Delta I_{jk}\, dI_{ij} = c\rho_{ij}\rho_{jk}, \quad (6)$$

where $c = (\delta^2 + 2I_{pq}^{(0)}\delta)/2$. Substituting (5), (6) into ΔE_{ij}, and adding initial energy $E_{ij}^{(0)}$, we get

$$E_{ij} = E_{ij}^{(0)} + \delta \left(\frac{dE_{ij}}{dI_{ij}}\right)^{(0)} \rho_{ij} - c\left(\frac{1}{m_j} + \frac{1}{m_i}\right)\rho_{ij}^2 + \frac{c\rho_{ij}}{m_j}\left(\sum_{\substack{k\neq i \\ k\in\mathbb{C}_j}} \rho_{jk}(\hat{\boldsymbol{n}}_{jk}\hat{\boldsymbol{n}}_{ij})\right) - \frac{c\rho_{ij}}{m_i}\left(\sum_{\substack{k\neq j \\ k\in\mathbb{C}_i}} \rho_{ik}(\hat{\boldsymbol{n}}_{ik}\hat{\boldsymbol{n}}_{ij})\right) + \alpha_{ij}(e_{ij}^2 - 1)E_{ijmax}. \quad (7)$$

Squaring both sides of equation (4) and then plugging in (7), we get a systems of equations:

$$\frac{k_{pq}}{k_{ij}}\rho_{ij}^2 E_{pq} = E_{ij}, \quad \{i,j\} \in \mathbb{P}. \quad (8)$$

In the above system, ρ_{ij}, $\{i,j\} \in \mathbb{P}$, are the variables. The energy E_{ij} is a polynomial of degree at most two, while E_{pq} has degree at most one. Thus, every equation in (8) is at most a cubic polynomial. Newton's method can be applied to solve this non-linear system, with the initial guesses of 1 for ρ_{pq}, where $\{p,q\}$ is the contact yielding the primary impulse, and of 0 for ρ_{ij}, for any $\{i,j\} \neq \{p,q\}$. In the first round of initialization, if any ρ_{ij} exceeds 1, set the primary contact $\{p,q\}$ to be such $\{i,j\}$ that has the biggest ρ_{ij} value. With the updated primary impulse pair, the system should now be solved again to finish the initialization. This process ensures the biggest variable stay as the denominator in the differential relationships, which improves numerical stability.

B. Numerical integration

After initialization of $\rho_{ij}^{(0)}$, numerical integration is performed as follows. At the nth step, increment the primary impulse I_{pq} by δ, and make the updates below:

$$\rho_{ij}^{(n)} = \sigma_{ij}\sigma_{pq}\sqrt{\frac{k_{ij}E_{ij}^{(n-1)}}{k_{pq}E_{pq}^{(n-1)}}}, \quad (9)$$

$$I_{ij}^{(n)} = I_{ij}^{(n-1)} + \delta\rho_{ij}^{(n)}, \quad (10)$$

$$E_{ij}^{(n)} = E_{ij}^{(n-1)} + \delta\rho_{ij}^{(n)}\left(\frac{dE_{ij}}{dI_{ij}}\right)^{(n)}, \quad (11)$$

where $\left(\frac{dE_{ij}}{dI_{ij}}\right)^{(n-1)}$ is evaluated according to (3). In the step, the ball velocities are computed from (1). Algorithm 1 summarizes the above procedure.

C. Example

A Newton's cradle consists of five identical balls with mass m and radius r aligned in a row. Each ball is hanged by a string of length l. Denote by e the coefficient of restitution between two balls. See Fig. 2. Usually one drags the left end ball to a certain height and then releases it. Several multi-body collisions will happen after the release. Every ball carries out a simple pendulum motion before it collides with another ball. The angle $\theta(t)$ between the perpendicular direction and the string at time t satisfies a second order ordinary differential equation. When it is small, under the approximation $\sin\theta \approx \theta$, the angle has a solution in the form of $\theta(t) = A\cos(\omega t + \phi)$, where $\omega = \sqrt{g/l}$ with g as the gravitational acceleration constant. The constants A and ϕ can be determined from the initial configuration at time $t = t_0$: the angle θ_0 of the pendulum and the tangential velocity v_0 as shown in Fig. 2. We obtain

$$\theta(t) = \sqrt{\theta_0^2 + \frac{v_0^2}{gl}}\cos(\omega t + \beta_0 - \omega t_0),$$

$$v(t) = -\sqrt{\theta_0^2 + \frac{v_0^2}{gl}}\sqrt{gl}\sin(\omega t + \beta_0 - \omega t_0).$$

Algorithm 1 Frictionless collision for n balls with translation only

Input: $\mathcal{B}_i$ with velocities $\boldsymbol{v}_i^{(0)}$, $1 \le i \le n$, and contact set $\mathbb{P}$

```
set the active contact set 𝔸 = ℙ
while 𝔸 ≠ ∅ do
    solve ρ_ij from the system (8), update I_ij, E_ij according to (10) and (11), also v_i, 1 ≤ i ≤ n according to (1)
    while 𝔸 does not change do
        update ρ_ij, I_ij, E_ij, for all {i,j} ∈ 𝔸 and v_i, 1 ≤ i ≤ n according to (9)–(11), and (1)
        for every {i,j} ∈ 𝔸 do
            if compression ends then
                add energy loss to E_ij
            else if restitution ends then
                remove the contact {i,j} from 𝔸
            end if
        end for
        for every {i,j} ∈ ℙ \ 𝔸 that v_i = v_j do
            add the contact {i,j} to 𝔸
        end for
    end while
end while
```

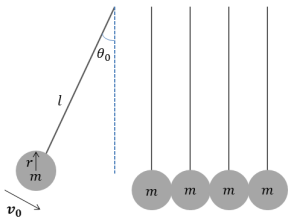

Fig. 2: Newton's cradle.

where β_0 is a constant offset determined by θ_0, v_0, g, and l. As time goes by, collisions are detected by checking if several balls are close enough with non-negligible relative velocities. Each ball may switch to a different simple pendulum motion due to the next collision which results in a sudden change of velocity. Algorithm 1 is applied to compute the motion of the balls for each collision. Simulation and experimental results will be shown in section IV-A.

III. Collision under General Motions with Friction

In this section, we will extend the impact model by considering friction and angular velocity of arbitrary shape objects in the system of collision treated in Section II. As before, the objects involved in the collision are assumed to have their centers of mass lying on the same plane. Besides, for every pair of contacting objects, we assume the contacting point and the centers of mass lie on the same line for simplicity reason. Section V will discuss how the assumption can be removed.

Denote by $\boldsymbol{v}_i$ and $\boldsymbol{\omega}_i$ the velocity and angular velocity of the object $\mathcal{B}_i$ in the world frame. At the moment of collision, let $\boldsymbol{r}_{ik}$ be the vector from $\mathcal{B}_i$'s center of mass to the contact point between $\mathcal{B}_i$ and $\mathcal{B}_k$. The angular inertia matrix Q_i of $\mathcal{B}_i$ is diagonal in its principal frame, which has undergone a rotation described by the matrix R_i from the world frame. For instance, if $\mathcal{B}_i$ is a ball with radius τ, then $Q_i = \frac{2}{5}m_i\tau^2 I_3$, where I_3 is the 3 by 3 identity matrix. In the world frame, the changes in the velocities and angular velocities of $\mathcal{B}_i$, $i = 1, ..., n$, during the impact can be derived from dynamics:

$$m_i \Delta \boldsymbol{v}_i = \sum_{k\in\mathbb{C}_i} \boldsymbol{I}_{ik}, \tag{12}$$

$$Q_i\left(R_i^{-1}\Delta\boldsymbol{\omega}_i\right) = \sum_{k\in\mathbb{C}_i} R_i^{-1}(\boldsymbol{r}_{ik}\times\boldsymbol{I}_{ik}). \tag{13}$$

Compared with the frictionless case studied in Section II, impulse now exists in the tangent plane at the contact between two objects. Here, let $I_{ik\perp}$ be the magnitude of the tangential impulse between $\mathcal{B}_i$ and $\mathcal{B}_k$ shown in Fig. 3, which is the projection of the total impulse $\boldsymbol{I}_{ik}$, exerted by $\mathcal{B}_k$ on $\mathcal{B}_i$, onto tangential plane. The component of $I_{ij\perp}$ in the x-y plane is I_{iku}, and the vertical component in z-direction is I_{ikz}. Compared to equation (2), we now have

$$\begin{pmatrix} v_{ix} \\ v_{iy} \end{pmatrix} = \begin{pmatrix} v_{ix}^{(0)} \\ v_{iy}^{(0)} \end{pmatrix} + \frac{1}{m_i}\sum_{k\in\mathbb{C}_i}\begin{pmatrix} I_{ikn}\cos\theta_{ik} - I_{iku}\sin\theta_{ik} \\ I_{ikn}\sin\theta_{ik} + I_{iku}\cos\theta_{ik} \end{pmatrix}. \tag{14}$$

The differential relationship between the energy and normal impulse at the contact between object $\mathcal{B}_i$ and $\mathcal{B}_j$ is

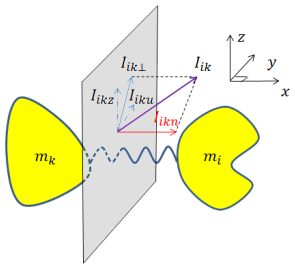

Fig. 3: Impulse decomposition along normal and tangential directions.

$$\begin{aligned}\frac{dE_{ij}}{dI_{ijn}} &= \cos\theta_{ij}\left(v_{jx}^{(0)} - v_{ix}^{(0)}\right) + \sin\theta_{ij}\left(v_{jy}^{(0)} - v_{iy}^{(0)}\right) \\ &+ \frac{1}{m_j}\sum_{k\in\mathbb{C}_j}\left(I_{jkn}\cos\left(\theta_{jk}-\theta_{ij}\right)\right. \\ &\left. - I_{jku}\sin\left(\theta_{jk}-\theta_{ij}\right)\right) \\ &- \frac{1}{m_i}\sum_{k\in\mathbb{C}_i}\left(I_{ikn}\cos\left(\theta_{ik}-\theta_{ij}\right)\right. \\ &\left. - I_{iku}\sin\left(\theta_{ik}-\theta_{ij}\right)\right).\end{aligned} \tag{15}$$

The variable ρ_{ij} defined in (4) for the frictionless case is now replaced by ρ_{ijn}, whose initial value will still be solved from the system of equations using Newton's method. An expression for E_{ij} can be derived by integrating equation (15) similarly as in Section II.

During the impact, we need to consider the contact mode (stick or slip) between $\mathcal{B}_i$ and $\mathcal{B}_j$. Denote by $\hat{\boldsymbol{n}}_{ij}$ the unit normal of the tangent plane between these two objects. The velocity of $\mathcal{B}_i$ relative to that of object $\mathcal{B}_j$ at the contact is $\Delta\boldsymbol{v}_{ij} = \boldsymbol{v}_i - \boldsymbol{v}_j + \boldsymbol{\omega}_i\times\boldsymbol{r}_{ij} - \boldsymbol{\omega}_j\times\boldsymbol{r}_{ji}$.

Project $\Delta\boldsymbol{v}_{ij}$ onto tangent plane to get $\Delta\bar{\boldsymbol{v}}_{ij} = \Delta\boldsymbol{v}_{ij} - \Delta\boldsymbol{v}_{ij}\cdot\hat{\boldsymbol{n}}_{ij}$. After simplification, the right hand side of the above equation can be written as linear combinations of ΔI_{ijn}, ΔI_{iju}, and ΔI_{ijz}.

The contacts among the n objects can be either sliding or sticking. We denote the set of sliding contacts as $\mathbb{S}$, and the set of sticking contacts as $\mathbb{T}$. The elements in each set are the pairs of indices for objects engaged in the corresponding contact mode. Clearly, $\mathbb{P} = \mathbb{S}\cup\mathbb{T}$. If the contact $\{i,j\}$ sticks, their relative velocities in the tangent plane should all be zero, i.e.,

$$\Delta\bar{\boldsymbol{v}}_{ij} = 0, \quad \{i,j\}\in\mathbb{T}. \tag{16}$$

Let $|\mathbb{T}|$ be the size of the set $\mathbb{T}$. The above equations form a linear system with $3|\mathbb{T}|$ equations and $3|\mathbb{T}|$ variables. Each $\Delta\bar{\boldsymbol{v}}_{ij}$ has three components along the x-, y- and z-axes, and also each equation has $3|\mathbb{T}|$ variables ΔI_{ijn}, ΔI_{iju}, and ΔI_{ijz}, $\{i,j\}\in\mathbb{T}$.

After solving the system, one can check the ratio γ_{ij} between the tangential impulse and the normal impulse

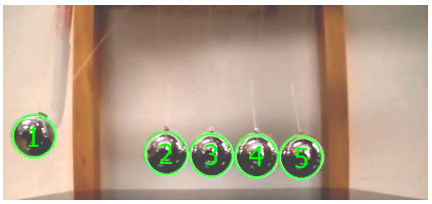

Fig. 4: Initial State of Newton's cradle. Green circles mark the contours of the five balls, which are numbered 1 to 5 from left to right.

at the contact $\{i, j\}$, that is $\gamma_{ij} = \Delta I_{ij\perp}/\Delta I_{ijn}$. Denote μ_{ij} as the coefficient of friction between $\mathcal{B}_i$ and $\mathcal{B}_j$. If $\gamma_{ij} \geq \mu_{ij}$, then sliding happens between $\mathcal{B}_i$ and $\mathcal{B}_j$. According to Coulomb's friction law, we set

$$\Delta I_{ij\perp} = \mu_{ij} \Delta I_{ijn}. \tag{17}$$

The values of ΔI_{iju} and ΔI_{ijz} are determined by the sliding direction, which is opposite to the relative velocity. If $\gamma_{ij} < \mu_{ij}$, we still have

$$\Delta I_{ij\perp} = \gamma_{ij} \Delta I_{ijn}. \tag{18}$$

Next, we perform numerical integration to update all the impulses, energies, velocities, and angular velocities. The computation is very similar to Algorithm 1, except that we are now using equations (12)-(18), and sliding or sticking mode will be involved as discussed above. Simulation results of nine-ball break shots will be presented in Section IV-B.

IV. Simulation and Experiment

Simulation and experiments on chains of aligned balls have been conducted in the past [10, 11]. In this section, we first present simulation of Newton's cradle by applying the frictionless model described in Section II, and compare the results with those from an experiment that we also conducted. Next, we present simulation of nine-ball break shots using the model in Section III.

A. Newton's cradle

To experimentally validate Algorithm 1, a Newton's Cradle with string length $l = 0.129$m was placed on a horizontal table. The five identical balls of the cradle have radius $r = 0.011$m, and between any two balls, the coefficient of restitution $e = 0.95$ and the stiffness is the same. The leftmost ball was initially raised and held static with an oscillation angle $5\pi/36$ as shown in Fig. 4. From the release, a video was captured by a Fujifilm FinePix HS10 camera with frame rate 30fps. The Hough Circle Transform algorithm [15] in Matlab was applied to track the contours of the five balls during their motions. Velocities were estimated based on the tracked ball positions and the frame rate.

Table I compares the horizontal velocities v_x and $\tilde{v}_x$ (m/s), in the experiment and simulation, respectively, of the five balls right after they were disengaged from the first collision. Interestingly, ball 1 was moving leftward slightly, and ball 4 was moving rightward at noticeable velocity in both the experiment and simulation. This phenomenon cannot be explained just based on conservation of momentum and energy. .

ball	1	2	3	4	5
v_x	-0.0578	-0.0224	0.0003	0.1322	0.4508
$\tilde{v}_x$	-0.0568	-0.0380	-0.0002	0.1450	0.4401

TABLE I: Comparisons of experimental (second row) and simulation (third row) outcomes from the first collision of the five balls. Listed are the ball velocities in the x-direction.

The experimental and simulation results are also compared along the time axis until no more impact happened so all the balls swung together. Fig. 5 compares the time trajectories of the horizontal velocities of ball 1 observed in the experiment and predicted by simulation. The two trajectories match very well, except that during every cycle (example shown in the inset) the ball velocity fluctuates slightly more in simulation than in the experiment. This is mainly due to some sticking effect between the balls in the experiment that is not modeled by Algorithm 1.

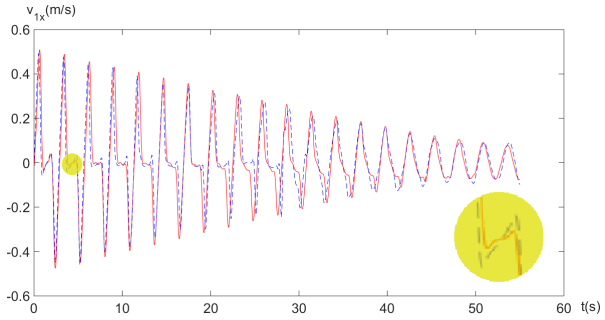

Fig. 5: Time trajectories of the horizontal velocity of Newton's cradle: experiment (red line) vs. simulation (blue dashed line).

B. Billiard break shots

Nine-ball break shots is a good test bed for the frictional model described in Section III. There are ten identical balls (including a cue ball) on the pool table with radius r and mass m. The initial configuration is shown in Fig. 6. The cue stick shoots the cue ball to generate initial velocity $\boldsymbol{v}_0$ and angular velocity $\boldsymbol{\omega}_0$. The

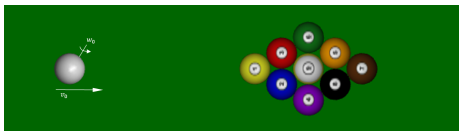

Fig. 6: Initial state of nine-ball break shot. The cue ball (white) is at the leftmost position.

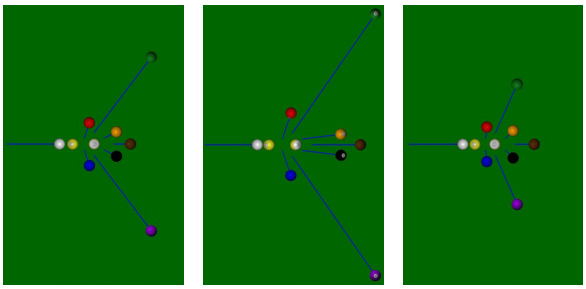

(a) (b) (c)

Fig. 7: Resting configurations of ten balls after three break shots: (a) stop shot, (b) follow shot, and (c) draw shot.

coefficient of friction between any two balls is the same, and denoted as μ_{bb}. Friction between a ball and the table is ignored during the impact. After the shot, the balls will be moving under sliding or rolling friction with the table, where μ_{bt} and $\tilde{\mu}_{bt}$ are the respective frictional coefficients. We applied the technique in [6] to compute the ball trajectories under given initial velocities and angular velocities.

The model in Section III is implemented to simulate break shots with parameters listed in Table II. Fig. 7 compares the final configurations following three different shots at the cue ball: stop shot, follow shot and draw shot. Immediately after the shots, the cue ball gains the same initial velocity $(1, 0, 0)$, but angular velocities $(0, 0, 0)$, $(0, 20, 0)$, and $(0, -20, 0)$, respectively. The results show that compared to a stop shot, the balls tend to spread out more under a follow shot and less under a draw shot.

d_b (m)	m_b (kg)	μ_{bb}	e_{bb}	μ_{bt}	$\tilde{\mu}_{bt}$
0.06	0.17	0.03	0.96	0.2	0.01

TABLE II: Parameters used for modeling break shots include d_b, the diameter of the balls; m_b, the mass of the balls; μ_{bb}, the ball-ball coefficient of friction; e_{bb}, the ball coefficient of restitution; μ_{bt}, the ball-table coefficient of friction; and $\tilde{\mu}_{bt}$, the ball-table coefficient of rolling resistance.

V. Discussion and Future Work

We have presented an n-body impact model in both frictionless and frictional cases. An assumption of the mass centers of the objects being coplanar has been made. However, the model is easily extendable to a general configuration with modifications of equations (14) and (15) to take into account the z-direction components. The formulas after integration will be more complex.

An immediate next step is to carry out simulation and experiment over general shapes. A billiard experiment in the near future is being planned for further model validation with the use of a vision system for velocity measurements. Efficiency of the algorithm can be improved after gaining better understanding of some numerical methods. Later on, we will be investigating path planning issues for a robot to play billiards skillfully.

VI. Acknowledgment

Support of this research was provided in part by Iowa State University (ISU), and in part by the National Science Foundation through the grant IIS-1421034. The authors would like to thank Benjamin Kollasch for his help on the experiment with Newton's cradle. Any opinions, findings and thoughts discussed in this material are those of the authors and do not necessarily reflect the views of the National Science Foundation.

References

[1] V. Acary and B. Brogliato. Concurrent multiple impacts modelling: Case-study of a 3-ball chain. In *Comp. Fluid and Solid Mech. Sec. Mit Conf.* Elsevier, 2003.

[2] V. Ceanga and Y. Hurmuzlu. A new look at an old problem: Newtons cradle. *J. appl. mech.*, 68(4):575–583, 2001.

[3] S. Hirai, M. Niwa, and S. Kawamura. Development of impulsive object sorting device with air floating. *In Proc. IEEE Int. Conf. Robot. Automat.,pp. 3065–3070*, 1999.

[4] W. H. Huang and M. T. Mason. Mechanics, planning, and control for tapping. *Int. J. Robot. Res.*, 19(10):883–894, 2000.

[5] Y. Jia. Three-dimensional impact: energy-based modeling of tangential compliance. *Int. J. Robot. Res.*, 32(1):56–83, 2012.

[6] Y. Jia. Planning the motion of a sliding and rolling sphere under friction. *In Proc. IEEE Int. Conf. Robot. Automat.,pp. 2396-2402, Seattle, WA*, 2015.

[7] Y. Jia, M. Mason, and M. Erdmann. Multiple impacts: A state transition diagram approach. *Int. J. Robot. Res.*, 32(1):84–114, 2012.

[8] C. Liu, Z. Zhao, and B. Brogliato. Frictionless multiple impacts in multibody systems. i. theoretical framework. *Proc. Royal Soc. A: Math. Phys. Engr. Sci.*, 464(2100):3193–3211, 2008.

[9] C. Liu, Z. Zhao, and B. Brogliato. Frictionless multiple impacts in multibody systems. ii. numerical algorithm and simulation results. *Proc. Royal Soc. A: Math. Phys. Engr. Sci.*, 465(2101):1–23, 2009.

[10] N. S. Nguyen and B. Brogliato. Shock dynamics in granular chains: numerical simulations and comparison with experimental tests. *Granular Matter*, 14(3):341–362, 2012.

[11] N.S. Nguyen and B. Brogliato. *Multiple impacts in dissipative granular chains*. Springer, 2014.

[12] W. Stronge. *Impact mechanics*. Cambridge university press, 2004.

[13] K. Tagawa, K. Hirota, and M. Hirose. *Manipulation of dynamically deformable object using impulse-based approach*. INTECH Open Access Publisher, 2010.

[14] Y. Wang, V. Kumar, and J. Abel. Dynamics of rigid bodies undergoing multiple frictional contacts. *In Proc. IEEE Int. Conf. Robot. Automat.,pp. 2764–2769*, 1992.

[15] H. K. Yuen, J. Princen, J. Illingworth, and J. Kittler. Comparative study of hough transform methods for circle finding. *Img. and vis. comp.*, 8(1):71–77, 1990.

[16] Brogliato B. Zhang, H. and C. Liu. Dynamics of planar rocking-blocks with coulomb friction and unilateral constraints: comparisons between experimental and numerical data. *Mult. Sys. Dynam.*, 32(1):1–25, 2014.

[17] Liu C. Zhao, Z. and B. Brogliato. Planar dynamics of a rigid body system with frictional impacts. ii. qualitative analysis and numerical simulations. *Proc. Royal Soc. A: Math. Phys. Engr. Sci.*, 465(2107):2267–2292, 2009.